Earth and Planetary Science Letters 491 (2018) 43–47

Contents lists available at ScienceDirect

Earth and Planetary Science Letters

www.elsevier.com/locate/epsl

Variations in the long-term uplift rate due to the Altiplano–Puna magma body observed with Sentinel-1 interferometry

Nicholas Lau *, Ekaterina Tymofyeyeva, Yuri Fialko

Institute of Geophysics and Planetary Physics, Scripps Institution of Oceanography, University of California, San Diego, La Jolla, CA 92093, USA

ARTICLE INFO

Article history:
Received 13 November 2017
Received in revised form 8 March 2018
Accepted 13 March 2018
Available online xxxx
Editor: R. Bendick

Keywords:
Altiplano
magma
diapir
uplift
InSAR

ABSTRACT

We present new Interferometric Synthetic Aperture Radar (InSAR) observations of surface deformation in the Altiplano–Puna region (South America) where previous studies documented a broad uplift at an average rate of ~10 mm/yr. We use data from the Sentinel-1 satellite mission to produce high-resolution velocity maps and time series of surface displacements between years 2014–2017. The data reveal that the uplift has slowed down substantially compared to the 1992–2010 epoch and is characterized by short-term fluctuations on time scales of months to years. The observed variations in uplift rate may indicate a non-steady supply of melt and/or volatiles from the partially molten Altiplano–Puna Magma Body (APMB) into an incipient diapir forming in the roof of the APMB.

1. Introduction

The Altiplano–Puna plateau in the Andes (South America) hosts one of the world's largest and most active volcanic provinces, the Altiplano–Puna Volcanic Complex (APVC), which spans southern Bolivia, northern Chile, and northern Argentina, and includes more than 50 potentially active volcanos (e.g., Silva, 1989). Seismic observations have detected a large low-velocity anomaly in the mid-to-upper crust underneath the APVC referred to as the Altiplano–Puna Ultra-Low Velocity Zone (APULVZ) (Chmielowski et al., 1999; Zandt et al., 2003; Ward et al., 2017). The observed reduction in seismic velocities requires the presence of partial melt, making the APULVZ the largest known active magma body in the Earth's continental crust. Space geodetic observations revealed a ~75 km-wide zone of surface uplift in the middle of the APULVZ, with a peak near the dormant Uturuncu volcano (Pritchard and Simons, 2002; Sparks et al., 2008). Fialko and Pearse (2012) showed that the uplift occurred at a quasi-constant rate of ~10 mm/yr between 1992 and 2010, and was surrounded by a broad zone of subsidence occurring at a rate of a few mm/yr – an unusual pattern referred to as the "sombrero uplift". Gottsmann et al. (2017b) suggested that the uplifted persisted at the same rate over the last 50 yrs, based on leveling and campaign Global Positioning System (GPS) data.

Model-based interpretations of the observed surface deformation attribute the central uplift to a magmatic source in the middle crust at depth of ~15–20 km (Pritchard and Simons, 2004; Fialko and Pearse, 2012; Henderson and Pritchard, 2013; Hickey et al., 2013; Potro et al., 2013; Walter and Motagh, 2014), although particular mechanisms of magmatic unrest are still not well-understood. Fialko and Pearse (2012) argued that the inferred mid-crustal depth of the deformation source, the proximity to the partially molten Altiplano–Puna Magma Body (APMB), and the long duration and quasi-steady nature of uplift imply viscous deformation mechanisms in the source region. One such mechanism could involve the formation and growth of a large magmatic diapir (Fialko and Pearse, 2012). According to this model, the ballooning diapir causes the central uplift, while withdrawal of partial melt from the APMB into the diapir is responsible for the peripheral subsidence. The diapir model appears to be consistent with recent seismic (Jay et al., 2012; Ward et al., 2014), gravity (Potro et al., 2013), and electromagnetic (Comeau et al., 2016; Laumonier et al., 2017) observations, as well as earlier suggestions that large amounts of dacite melt may be transported in diapirs from the middle to the upper crust within the APVC proper (Silva, 1989). Gottsmann et al. (2017a) presented data from a continuous GPS site installed in 2010 near the center of uplift, showing variations in the uplift rate on sub-decadal time scales, and proposed that the observed surface deformation may result from cycles of pressurization and de-pressurization in a vertically-elongated magma reservoir connected to the APMB, similar to the incipient diapir geometry inferred by Fialko and Pearse (2012).

* Corresponding author.
E-mail address: h4lau@ucsd.edu (N. Lau).

https://doi.org/10.1016/j.epsl.2018.03.026
0012-821X/

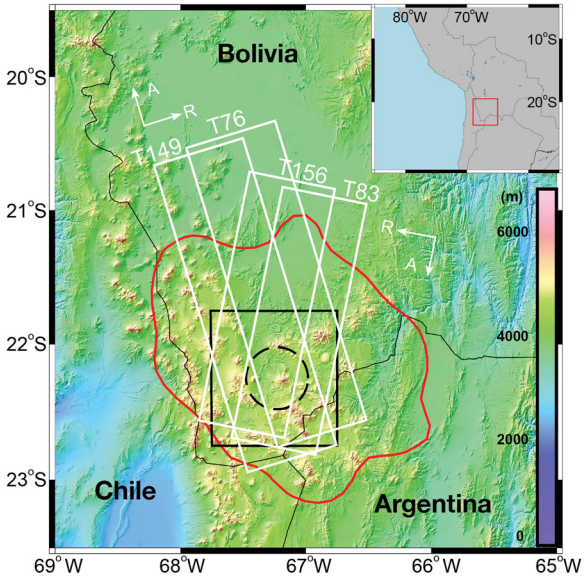

Fig. 1. Overview map of area of interest. Sub-swathes of Sentinel-1 data from ascending (76, 149) and descending (83, 156) tracks used in this study are denoted by white rectangles. Arrows denote satellite heading (azimuth, A) and line of sight (range, R) directions. Black dashed circle represents the spatial extent of uplift documented by previous studies (Fialko and Pearse, 2012; Henderson and Pritchard, 2013). Red line denotes the 2.9 km/s velocity contour outlining the seismically imaged extent of the low velocity zone at depth of 20 km (Ward et al., 2017). Black rectangle denotes area shown in Fig. 2. (For interpretation of the colors in the figure(s), the reader is referred to the web version of this article.)

In this paper, we present new Interferometric Synthetic Aperture Radar (InSAR) data that extend the time series of surface deformation in Altiplano–Puna to 25 yrs. The new observations reveal that the uplift rate has decreased over the last decade compared to the previous two decades, and that the rates of surface motion may indeed fluctuate on time scales on the order of months to years. We discuss implications from the observed time history of uplift for possible driving mechanisms.

2. Data and methods

We analyzed data acquired between September 2014 and December 2017 by the Sentinel-1A/B satellites. We used individual sub-swaths from ascending tracks 76, 149 and descending tracks 83, 156 (Fig. 1), covering the area of uplift imaged by the ERS-1/2 and Envisat observations between the years 1992 and 2010 (Pritchard and Simons, 2002; Fialko and Pearse, 2012; Henderson and Pritchard, 2013). The data were processed using the Generic Mapping Tools Synthetic Aperture Radar (GMTSAR) package (Sandwell et al., 2011). We produced interferograms for every pair of sequential acquisitions for each satellite track, resulting in a total of 215 interferometric pairs (see Figs. S1 and S2 of Supporting Information). Single look complex images were aligned using the Bivariate Enhanced Spectral Diversity (BESD) method (Wang et al., 2017). We used the Shuttle Radar Topography Mission (SRTM) 30 m resolution digital elevation model (DEM) (Farr and Kobrick, 2000) to remove the topographic contribution from the interferometric phase. Interferograms were unwrapped using the SNAPHU algorithm (Chen and Zebker, 2002). Short revisit times and tight orbital controls of the Sentinel-1 satellites, combined with arid low-vegetation surface conditions, result in high coherence of interferometric phase in the study area.

Propagation effects are known to be the main limitation to the accuracy of InSAR measurements of low-amplitude deformation (Tarayre and Massonnet, 1996; Fialko and Simons, 2001; Li et al., 2005; Foster et al., 2006; Ding et al., 2008). In particular, interferometric phase can be affected by variations in the electron content in the ionosphere, and water vapor in the troposphere. Tropospheric contributions consist in part of a turbulent component that is random in time and follows a power law distribution in space (e.g., Ding et al., 2008), and a stratified component that may or may not be systematic in time but is spatially correlated with topography (e.g., Doin et al., 2009). We estimated the propagation effects due to ionosphere and turbulent water vapor mixing in the troposphere using an iterative common-scene stacking method CANDIS (Tymofyeyeva and Fialko, 2015). The method takes advantage of frequent data acquisitions to estimate and remove the propagation artifacts, under the assumption of quasi-constant rates of surface deformation. The temporally random component of phase delays was calculated using a 200-day averaging stencil (see Tymofyeyeva and Fialko, 2015, for details). Figs. S1 and S2 in Supporting Information show the estimated atmospheric noise coefficients (a measure of the amplitude of propagation artifacts) for different acquisition dates.

After we applied the CANDIS correction, some interferograms exhibited a correlation between the unwrapped radar phase and topography, which could be attributed to residual propagation delays due to a stratified troposphere. These signals can vary systematically with time (e.g., due to seasonal variations in tropospheric water content), in which case they would not be removed by the common-point stacking method, as the latter preserves any variations in phase that are quasi-linear on a time scale of satellite revisits. To mitigate the seasonally-varying atmospheric noise, we combined sequential interferograms (corrected for the turbulent noise) to form a set of year-long interferograms that begin and end on the same month of a year. This resulted in ∼20 independent year-long interferograms for each track. We found that addition of sequential interferograms may introduce a high-frequency noise to the radar phase due to filtering artifacts. Therefore filtering and unwrapping can be applied after summation of individual raw interferograms. Interferograms with a time span of one year minimize seasonal differences in the net water vapor content in the troposphere, although may still be affected by longer-term (e.g. decadal) trends. Each one-year interferogram was subsequently "de-ramped", by subtracting the best-fit plane, to correct for any residual long-wavelength artifacts. We then estimated the remaining contributions due to the stratified water vapor in the atmosphere by regressing the line of sight (LOS) displacements against elevation (e.g., Bekaert et al., 2015). To prevent a potential bias due to surface deformation, we excluded data from the geodetically imaged uplift area (black dashed circle in Fig. 1). The observed dependence of LOS displacements on topography is illustrated in Fig. S3. After subtracting the best-fit linear scaling between phase and topography from the year-long interferograms, we computed the mean LOS velocities by averaging the corrected year-long interferograms for each track and dividing by the respective time interval. Averaging is expected to further suppress any residual random noise by a factor of $\sqrt{N}$ given N independent samples (e.g., Zebker et al., 1997; Fialko, 2006). The results are shown in Fig. 2. We also computed time series of LOS displacements from the original set of sequential interferograms corrected for the turbulent atmospheric noise (Tymofyeyeva and Fialko, 2015).

3. Results

Fig. 3 shows a profile of the mean LOS velocities from the four Sentinel-1 tracks spanning the uplift area (Fig. 2). For comparison, we also include the mean LOS velocities from the same profile corresponding to the previous ∼20 yrs (1992–2010; orange dots in Fig. 3). While the LOS velocities derived from Sentinel-1 data are still noisy because of the relatively short observation period, they consistently indicate that the uplift rate over the last 3 yrs